

1

**SUPPLEMENTARY MATERIAL**

2

3

**The potential of MOF accelerator in**

4

**electrochemiluminescence system for sensitivity detection**

5

**of menthol enantiomers**

6

7

Xuan Kuang <sup>a\*</sup>, Yeqian Ruan <sup>a</sup>, Jianping Xin <sup>b</sup> and Lin Lan <sup>a\*</sup>

8

9

10

<sup>a</sup> Key Laboratory of Interfacial Reaction & Sensing Analysis in Universities of

11

Shandong, School of Chemistry and Chemical Engineering, University of Jinan,

12

Jinan 250022, China

13

<sup>b</sup> Shandong Institute of Non-Metallic Materials, Jinan 250031, China

14

15

16

1

## Table of Contents

### 2 1. Experiment section

#### 3 1.1 Reagents and Apparatus

#### 4 1.2 Characterisation of Circular dichroism spectra

#### 5 1.3 The calculation of ECL efficiency

#### 6 1.4 The calculation of detection limit

### 7 2. Figure and Table

8 **Figure S1.** UV-vis absorption (blue) and FL emission spectrum (orange) of L-  
9 CdS QDs

10 **Figure S2.** Cyclic voltammograms and Nyquist plots

11 **Figure S3.** Circular dichroism spectra of  $\beta$ -CD and  $\beta$ -CD + L-/D-Men

12 **Figure S4.** Condition optimization

13 **Figure S5.** Specificity of the ECL system

14 **Figure S6.** Application of the enantioselective electrode

15 **Table S1.** Comparison of ECL method with other reported methods

### 16 3. References

## 1. Experiment section

**1.1 Reagents and Apparatus.** The reagents were obtained from commercial sources and used directly without further purification. The reagents are analytical grade.  $\text{CdCl}_2 \cdot 2.5\text{H}_2\text{O}$ ,  $\text{Na}_2\text{S} \cdot 9\text{H}_2\text{O}$ ,  $\text{Zn}(\text{NO}_3)_2 \cdot 6\text{H}_2\text{O}$ , Triethylamine (TEA), 2-Methylimidazole (Hmim), L-aspartic acid (L-Asp), L-/D-menthol (L-/D-Men), L-/D-tyrosine (L-/D-Tyr), L-/D-arginine (L-/D-Arg), L-/D-tryptophan (L-/D-Trp), L-/D-glutamic acid (L-/D-Glu), L-/D-proline (L-/D-Pro), L-/D-threonine (L-/D-Thr), L-/D-histidine (L-/D-His), L-/D-serine (L-/D-Ser), L-/D-methionine (L-/D-Met), R-/S-mandelic acid (R-/S-Man), L-/D-phenylalanine (L-/D-Phe), L-/D-valine (L-/D-Val), L-/D-alanine (L-/D-Ala), L-/D-carnitine (L-/D-Car), L-/D-penicillamine (L-/D-PA), R-/S-naproxen (R-/S-Nap), potassium dihydrogen phosphate ( $\text{KH}_2\text{PO}_4$ ), disodium hydrogen phosphate ( $\text{Na}_2\text{HPO}_4$ ) and potassium chloride (KCl) were purchased from Sigma Aldrich (Shanghai, China). Methanol and ethanol were obtained from Tianjin Fuyu Fine Chemical Co, Ltd. All aqueous solutions were prepared with ultrapure water (DW, 18.25 M $\Omega$ .cm).

Scanning electron microscopy (SEM) images were characterized by a FEI QUANTA FEG250 transmission electron microscope at 15.0 kV. Powder X-ray patterns (PXRD) of samples were measured on a Bruker SMART APEX chargecoupled device (CCD)-based diffractometer using Cu K $\alpha$  radiation ( $\lambda = 1.5418 \text{ \AA}$ ) at room temperature (298 K). Fourier transform infrared (FT-IR) spectroscopy (KBr pellets) of materials was recorded on a Nicolet iS50 spectrometer. Electrochemical impedance analysis (EIS) was carried out in 0.1 M KCl aqueous solution containing  $\text{Fe}(\text{CN})_6^{3-/4-}$  as a redox marker with

1 scanning frequencies ranging from 1 to  $10^5$  Hz. ECL measurements were  
2 performed on an HYZ-3002 ECL analyzer obtained from Zhengzhou Shirui  
3 Instrument Technology Co., Ltd (Xi'an, China), and the experimental  
4 parameters were listed as follows: a photomultiplier voltage of 500 V, a scan  
5 rate of  $200 \text{ mV s}^{-1}$ , and a potential ranging from  $-1.6$  to  $0 \text{ V}$  (vs Ag/AgCl).

6 **1.2 Characterisation of Circular dichroism spectra.** To further validate the  
7 adsorption of Men isomers by cyclodextrins, we continued to characterise the  
8 experiments with Circular dichroism (CD). Two portions of  $\beta$ -CD (10 mM) were  
9 taken and dissolved in water, followed by the addition of an equal amount of  
10 aqueous L-/D-Men (10 mM) solution dissolved in water, respectively, and after  
11 twenty minutes of adsorption, the  $\beta$ -CD was rotary distilled and washed with  
12 EtOH to remove any remnants adsorption. After drying, equal amounts of the  
13 above solid and  $\beta$ -CD (1 mg/mL) were dissolved in water and their CD signals  
14 were measured.

15 **1.3 The calculation of ECL efficiency.** The calculation of ECL efficiency. The  
16 ECL value refers to the ECL efficiency of  $\text{Ru}(\text{bpy})_3\text{Cl}_2/\text{K}_2\text{S}_2\text{O}_8$  using the  
17 following formula<sup>1-3</sup>:

$$\Phi_{ECL} = \frac{\left( \frac{\int ECL dt}{\int current dt} \right)_x}{\left( \frac{\int ECL dt}{\int current dt} \right)_{st}} \times 100\%$$

18

19 where "ECL intensity" and "current" represent the integration of ECL intensity  
20 and electrochemical current value from the cumulative ECL spectrum,

1 respectively, and “st” refers to the standard Ru(bpy)<sub>3</sub>Cl<sub>2</sub>/K<sub>2</sub>S<sub>2</sub>O<sub>8</sub>. Specifically,  
2  $\Phi_{st}$  is the ECL efficiency of 1 mM [Ru(bpy)<sub>3</sub>]<sup>2+</sup> in 0.1 M K<sub>2</sub>S<sub>2</sub>O<sub>8</sub>/PBS, which is  
3 be regarded as a standard, taken as 5.0%. According to calculations, the  
4 calculated ECL efficiency of the  $\beta$ -CD/L-CdS QDs/L-His-ZIF-8 system was  
5 34.7%.

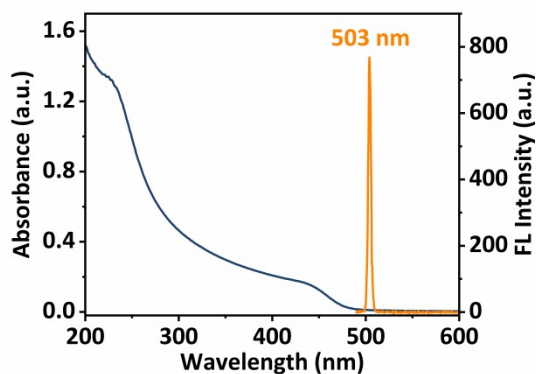
6 **1.4 The calculation of detection limit.** An ECL measurement for blank samples  
7 was implemented with ten parallel tests, which exhibited an average ECL  
8 intensity ( $I_B$ ) of 17416 with a standard deviation ( $S_B$ ) of 28.2.  $k$  was a numerical  
9 factor chosen according to the signal-to-noise ratio value and a value of 3 for it  
10 in the equation was strongly recommended. Therefore, the smallest detectable  
11 signal ( $I_L$ ) could be calculated as follows:

$$12 \quad I_L = I_B - k * S_B$$

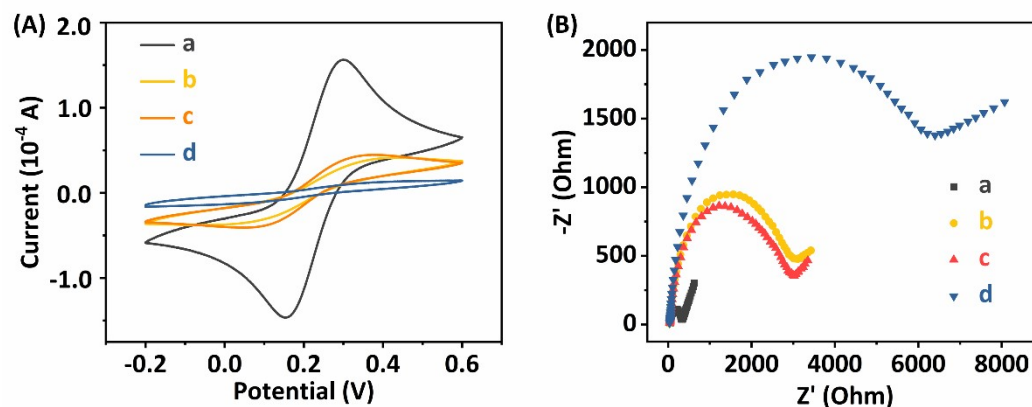
13 After that, by substituting  $I_L$  (17430.2) into the standard curve equation, the  
14 lowest detection limit of both L-Men and D-Men can be calculated, which was  
15 0.046  $\mu$ M.

16

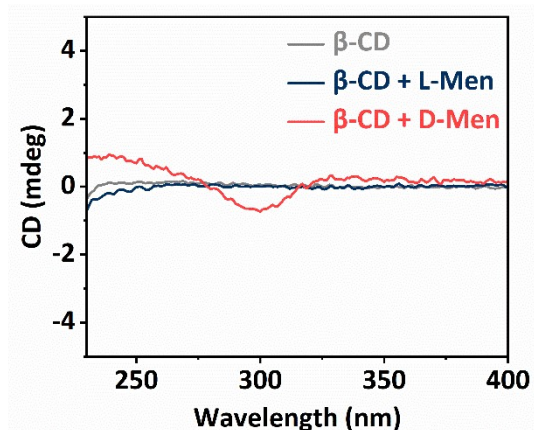
1 **2. Figure and Table**



7  
8 **Figure S1.** UV-vis absorption (blue) and FL emission spectrum (orange) of L-  
9 CdS QDs.



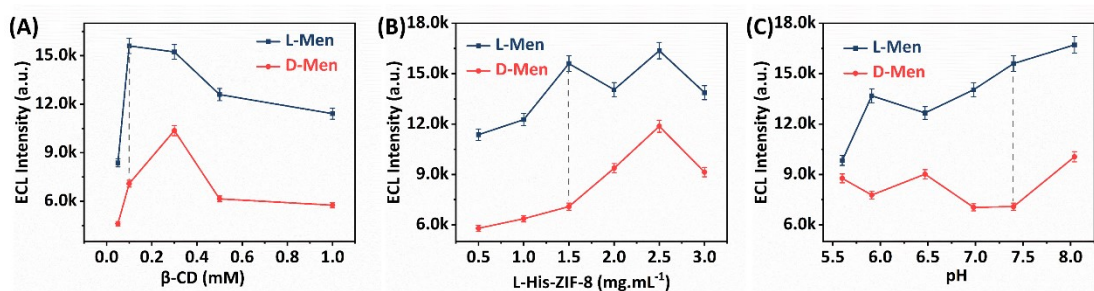
12 **Figure S2.** (A) Cyclic voltammograms and (B) Nyquist plots of (curve a) bare  
13 GCE, (curve b)  $\beta$ -CD/GCE, (curve c)  $\beta$ -CD/L-CdS QDs/GCE and (curve d)  $\beta$ -  
14 CD/L-CdS QDs/L-His-ZIF-8/GCE in 0.1 M KCl containing 5 mM  
15  $[\text{Fe}(\text{CN})_6]^{4-/3-}$ .



1

2 **Figure S3.** Circular dichroism of  $\beta$ -CD (grey),  $\beta$ -CD + L-Men (blue) and  $\beta$ -CD  
 3 + D-Men (red).

4



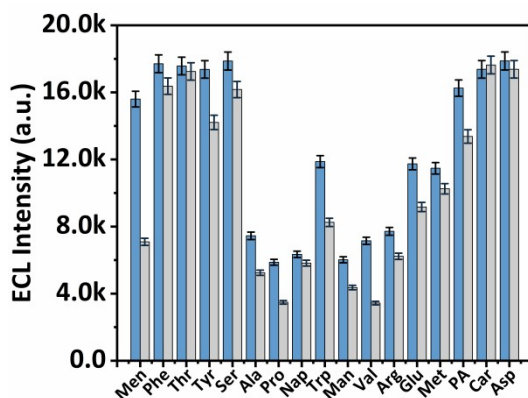
5

6 **Figure S4.** Influence of (A) the concentration of  $\beta$ -CD, (B) the concentration of  
 7 L-His-ZIF-8 and (C) pH on the ECL signals. Error bars are RSD ( $n = 3$ ).

8

9

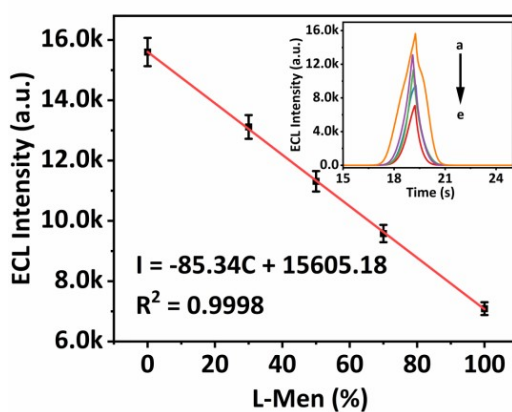
10



1

2 **Figure S5.** Comparison of enantioselectivity of enantiomers (0.1 mM) on the  $\beta$ -  
 3 CD/L-CdS QDs/L-His-ZIF-8/GCE + different amino acid enantiomers in PBS  
 4 (pH 7.4). Among them, the blue bar chart shows L-enantiomers, and the gray  
 5 bar chart shows D-enantiomers (except for Nap and Man, where the blue and  
 6 gray bar charts correspond to R and S enantiomers, respectively). Error bars are  
 7 RSD (n = 3).

8



9

10 **Figure S6.** The linear relationship between ECL signals and L-Men%. Inset:  
 11 ECL of 0.1 mM Men mixture containing different content of L-Men in the  
 12 mixture (0, 30, 50, 70 and 100%, corresponding to curves a to e) on  $\beta$ -CD/L-CdS  
 13 QDs/L-His-ZIF-8/GCE. Error bars are RSD (n = 3).



1 **Table S1.** Comparison of the performance of the proposed and referenced ECL chiral  
 2 sensors for enantiomers detection.

Anaiyte	Methods	Linear range	LOD	Reference
Glu	ECL	0.005-5.0 mM	1.6 $\mu$ M	4
Pro	ECL	0.001-1 mM	0.33 $\mu$ M	5
PA	ECL	2-12 mM	0.3 mM	6
Pen	ECL	0.1-5.0 mM	33 $\mu$ M	7
DAAO	ECL	0-10.0 mM	0.03 mM	8
Men	ECL	0.050-100 $\mu$ M	0.046 $\mu$ M	This work

3

### 3. References

1. J. Wang, Z. Han, T. Shang, Y. Feng, R. Liu and X. Lu, Artemisinin: a novel chiral electrochemiluminescence luminophore-assisted enantiospecific recognition and mechanism identification, *Chemical Science*, 2024, **15**, 5581-5588.
2. Y. Fang, Z. Zhou, Y. Hou, C. Wang, X. Cao, S. Liu, Y. Shen and Y. Zhang, Highly Efficient Wavelength-Resolved Electrochemiluminescence of Carbon Nitride Films for Ultrasensitive Multiplex MicroRNA Detection, *Analytical Chemistry*, 2023, **95**, 6620-6628.
3. J. Fang, L. Dai, R. Feng, D. Wu, X. Ren, W. Cao, H. Ma and Q. Wei, High-Performance Electrochemiluminescence of a Coordination-Driven J-Aggregate K-PTC MOF Regulated by Metal-Phenolic Nanoparticles for Biomarker Analysis, *Analytical Chemistry*, 2023, **95**, 1287-1293.
4. S. Zhu, X. Lin, P. Ran, F. Mo, Q. Xia and Y. Fu, A glassy carbon electrode modified with C-dots and silver nanoparticles for enzymatic electrochemiluminescent detection of glutamate enantiomers, *Microchimica Acta*, 2017, **184**, 4679-4684.
5. S. Zhu, P. Ran, J. Wu, M. Chen and Y. Fu, An Electrochemiluminescence Chiral Sensor for Propranolol Enantiomers Based on Functionalized Graphite-like Carbon Nitride Nanosheets, *Electroanalysis*, 2020, **32**, 185-190.

- 1       6. L. Lan, X. Song, X. Kuang, X. Sun and R. Kuang, Chiral Discrimination of  
2       Penicillamine Enantiomers: The Role of Aggregation-Caused Quenching in  
3       Achieving High Selectivity, *Analytical Chemistry*, 2023, **95**, 14659-14664.
- 4       7. X. Lin, S. Zhu, Q. Wang, Q. Xia, P. Ran and Y. Fu, Chiral recognition of  
5       penicillamine enantiomers using hemoglobin and gold nanoparticles  
6       functionalized graphite-like carbon nitride nanosheets via  
7       electrochemiluminescence, *Colloids and Surfaces B: Biointerfaces*, 2016,  
8       **148**, 371-376.
- 9       8. Q. Zhao, W. Zhu, W. Cai, J. Li, D. Wu and Y. Kong, TiO<sub>2</sub> Nanotubes  
10      Decorated with CdSe Quantum Dots: A Bifunctional  
11      Electrochemiluminescent Platform for Chiral Discrimination and Chiral  
12      Sensing, *Analytical Chemistry*, 2022, **94**, 9399-9406.